Measuring steady-state and dynamic endoplasmic reticulum and Golgi Zn^{2+} with genetically encoded sensors

Yan Qin, Philip J. Dittmer, J. Genevieve Park, Katarina B. Jansen, and Amy E. Palmer[1]

Department of Chemistry and Biochemistry, University of Colorado, Boulder, CO 80309

Edited* by Joan Selverstone Valentine, University of California, Los Angeles, CA, and approved March 22, 2011 (received for review October 19, 2010)

Zn^{2+} plays essential roles in biology, and cells have adopted exquisite mechanisms for regulating steady-state Zn^{2+} levels. Although much is known about total Zn^{2+} in cells, very little is known about its subcellular distribution. Yet defining the location of Zn^{2+} and how it changes with signaling events is essential for elucidating how cells regulate this essential ion. Here we create fluorescent sensors genetically targeted to the endoplasmic reticulum (ER) and Golgi to monitor steady-state Zn^{2+} levels as well as flux of Zn^{2+} into and out of these organelles. These studies reveal that ER and Golgi contain a concentration of free Zn^{2+} that is 100 times lower than the cytosol. Both organelles take up Zn^{2+} when cytosolic levels are elevated, suggesting that the ER and Golgi can sequester elevated cytosolic Zn^{2+} and thus have the potential to play a role in influencing Zn^{2+} toxicity. ER Zn^{2+} homeostasis is perturbed by small molecule antagonists of Ca^{2+} homeostasis and ER Zn^{2+} is released upon elevation of cytosolic Ca^{2+} pointing to potential exchange of these two ions across the ER. This study provides direct evidence that Ca^{2+} signaling can influence Zn^{2+} homeostasis and vice versa, that Zn^{2+} dynamics may modulate Ca^{2+} signaling.

zinc homeostasis | calcium signaling | zinc sensor | FRET

Zinc is the second most abundant transition metal in biological organisms, with mammalian cells containing an estimated 100–500 μM total Zn^{2+} (1, 2). The majority of this Zn^{2+} is bound to proteins and enzymes and indeed it has been estimated that approximately 10% of the human proteome or 3,200 proteins require zinc for their structure and function (3). It is now well established that mammalian cells contain a small but measurable pool of free or labile Zn^{2+} in the cytosol that is buffered in the picomolar range (4–6). Fluctuations in cytosolic Zn^{2+} have been shown to influence signaling cascades such as the mitogen activated protein kinase pathway (7), as well as cellular processes such as mitochondrial function (8, 9), apoptosis (10, 11), and dendritic cell maturation (12). Although many studies have focused on cytosolic Zn^{2+}, the overall distribution of zinc at the subcellular level is not well defined. In particular, it is not clear whether organelles contain labile Zn^{2+}, if so how these Zn^{2+} pools influence organelle function, and whether organelles modulate fluctuations in cytosolic Zn^{2+}. Yet defining where Zn^{2+} is located, whether it translocates from one place to another in response to stimuli, and how Zn^{2+} flux influences cellular processes is a fundamental part of elucidating how cells regulate and are influenced by this essential metal ion.

Mammalian cells contain an elaborate network of Zn^{2+} transporters, including 10 ZnT/cation diffusion facilitator (SLC30) family members and 14 Zrt-, Irt-like protein (SLC39) family members (13). These transporters help mediate zinc flux into and out of the cell and intracellular organelles. It is well established that Zn^{2+} can be concentrated into secretory vesicles (14), and recent studies have demonstrated a labile pool of Zn^{2+} in mitochondria (9, 15, 16), yet little is known about other intracellular organelles such as the endoplasmic reticulum (ER) and Golgi. Numerous proteins found within the secretory pathway require Zn^{2+} for their function, including resident ER chaperones such as calnexin and calreticulin, as well as secreted proteins such as metalloproteases and alkaline phosphatases (2). Moreover, deletion of an ER-localized ZnT in both yeast and higher eukaryotic cells led to activation of the unfolded protein response and general ER dysfunction (17, 18), suggesting Zn^{2+} plays an essential role in normal ER function.

In this work, we develop high-affinity genetically encoded Zn^{2+} sensors targeted to organelles to allow direct monitoring of ER and Golgi Zn^{2+} levels. These sensors reveal free Zn^{2+} in both the ER and Golgi at a concentration just under 1 pM. We demonstrate that the ER and Golgi sequester excess cytosolic Zn^{2+} indicating that organelles have the potential to play a role in modulating bioavailability of cytosolic Zn^{2+}. Moreover, using a combination of Ca^{2+} and Zn^{2+} sensors along with small molecule antagonists of calcium homeostasis, we discover a connection between ER Ca^{2+} stores and ER Zn^{2+} dynamics, providing evidence of interplay between Zn^{2+} homeostasis and Ca^{2+} signaling.

Results

Generation of High-Affinity Zn^{2+} Sensors Comprising Zap1, Cyan, and Yellow Fluorescent Proteins (ZapCY1 and ZapCY2). In this work, we optimized a sensor developed by Qiao et al. (19) which is comprised of the first and second zinc fingers of *Saccharomyces cerevisiae* Zap1 sandwiched between two fluorescent proteins [enhanced cyan fluorescent protein (CFP) and enhanced yellow fluorescent protein (EYFP)]. Zn^{2+} binding induces a conformational change in the pair of zinc fingers leading to an increase in FRET from CFP to YFP (Fig. 1*A*). In yeast suspensions of the original sensor, Zn^{2+} led to a 1.3-fold increase in the FRET ratio (R), defined as the FRET emission intensity divided by the CFP emission intensity (19). To optimize the sensor, we truncated CFP, replaced EYFP with the more pH stable citrine (20), and changed the amino acids in the linker regions to those found in Ca^{2+} sensors. Such changes have previously been shown to optimize the FRET response of genetically encoded calcium sensors (21). To characterize the sensor, which we named ZapCY1, we measured the apparent dissociation constant (K_d') of purified sensor protein in vitro. The Zn^{2+} binding curve was fit to a one-site saturation model yielding a $K_d' = 2.5$ pM (Fig. 1*B*). Titration with a series of metal ions revealed that ZapCY1 was selective for Zn^{2+} over other metal ions (Ca^{2+}, Mg^{2+}, Cu^{1+}, Cu^{2+}, Mn^{2+}, Co^{2+}, Ni^{2+}, Fe^{2+}) (Fig. 1*C* and *SI Appendix*, Fig. S1*A*). Only Zn^{2+} gave

Author contributions: Y.Q., P.J.D., and A.E.P. designed research; Y.Q., P.J.D., J.G.P., and K.B.J. performed research; Y.Q., P.J.D., and A.E.P. analyzed data; and Y.Q., P.J.D., and A.E.P. wrote the paper.

The authors declare no conflict of interest.

*This Direct Submission article had a prearranged editor.

Data deposition: The sequences reported in this paper have been deposited in the GenBank database, http://www.ncbi.nlm.nih.gov/genbank/ (accession nos. JF261177, JF261178, JF261179, and JF261180).

[1]To whom correspondence should be addressed. E-mail: amy.palmer@colorado.edu.

This article contains supporting information online at www.pnas.org/lookup/suppl/doi:10.1073/pnas.1015686108/-/DCSupplemental.

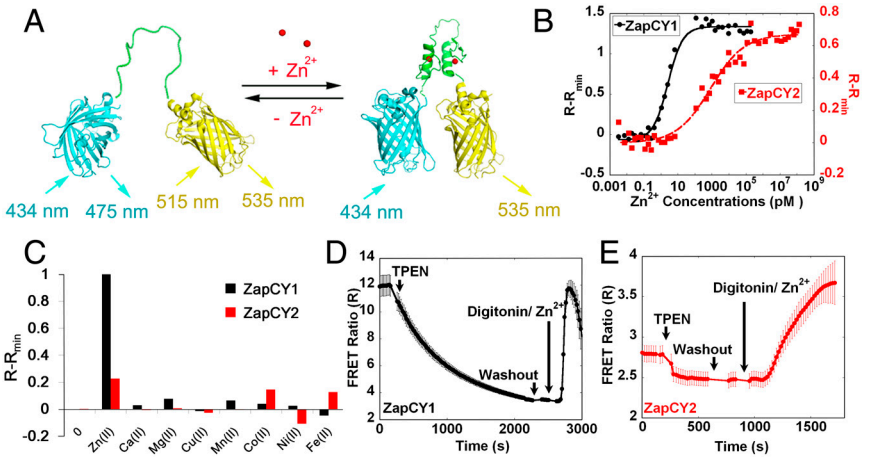

Fig. 1. Generation of high-affinity Zn^{2+} sensor ZapCY. (*A*) Schematic of the ZapCY sensor. (*B*) In vitro titration of ZapCY1 (●, K_d = 2.53 pM) and ZapCY2 (■, K_d = 811 pM, n = 0.44) sensor. (*C*) Metal selectivity of ZapCY1 and ZapCY2 sensor. Two micromolar ZapCY1 solutions were combined with 15 μM EDTA and 20 μM indicated metals, to yield 2:5 molar ratio of protein:metal. For ZapCY2, 1 μM metal was added to 2 μM sensor solutions to yield 2:1 solutions. Data represent the FRET ratio upon addition of a given metal minus the R_{min}. (*D*) Representative experiment (n = 5 cells) demonstrating changes in the FRET ratio of ZapCY1 in the cytosol of HeLa cells. (*E*) Representative experiment (n = 6 cells) demonstrating changes in the FRET ratio of ZapCY2 in the cytosol of HeLa cells. For *D* and *E*, FRET ratios differ from in vitro ratios due to different instrumentation and data processing. Microscope filter combinations for FRET and CFP: 430/24 excitation filter, 455 dichroic, 535/25, and 470/24 emission filters, respectively.

rise to a FRET ratio change when ZapCY1 protein was treated with excess metal ions. Because Ca^{2+} and Mg^{2+} are present at high concentrations in cells, we verified that micromolar concentrations of these ions do not perturb the sensor in vitro (*SI Appendix*, Fig. S1*C*) or in HeLa cells (*SI Appendix*, Fig. S2*E*). Treatment with neocuproine, a Cu^{1+} chelator, and 2,2-bipyridine, an Fe^{2+} chelator, had no effect on the sensor in HeLa cells, indicating that physiological Cu^{1+} and Fe^{2+} do not interfere with the sensor in cells under resting conditions (*SI Appendix*, Fig. S2). Fig. 1*D* demonstrates that ZapCY1 exhibits a large decrease in the FRET ratio when treated with a membrane permeable metal chelator *N*,*N*,*N*′,*N*′-tetrakis-(2-pyridylmethyl)-ethylenediamine (TPEN), followed by an increase upon saturation with Zn^{2+}, yielding the minimum and maximum ratio (R_{min} and R_{max}), respectively. In cells, ZapCY1 exhibits a 4.15-fold dynamic range (R_{max}/R_{min}) (Fig. 1*D*).

Mutation of two cysteines in the binding domain of ZapCY1 to histidine lowered the K_d′, generating another sensor ZapCY2. In vitro Zn^{2+} titration data fit equally well to an empirical Hill expression (K_d′ of 811 pM, n = 0.44, Fig. 1*B*) and a two-site saturation model (*SI Appendix, Methods*). This sensor yielded a 1.4-fold dynamic range in HeLa cells (Fig. 1*E*). Pseudocolored FRET ratio images of a representative titration are presented in *SI Appendix*, Fig. S3. ZapCY2 was less selective than ZapCY1 at a 2:5 molar ratio of protein:metal (*SI Appendix*, Fig. S1*D*), but was reasonably selective for Zn^{2+} at a 2:1 molar ratio (Fig. 1*C*). However, ZapCY2 was perturbed by Cu^{1+}, even at very low molar excesses in vitro (*SI Appendix*, Fig. S1*A*). Therefore, we tested whether Cu^{1+} was capable of influencing measurements of resting cytosolic Zn^{2+}; neocuproine had no effect on the resting FRET ratio, indicating that physiological Cu^{1+} does not perturb the sensor under resting conditions (*SI Appendix*, Fig. S2*D*). In addition, ZapCY2 was not perturbed by endogenous Fe^{2+} or micromolar levels of Ca^{2+} and Mg^{2+} in cells (*SI Appendix*, Figs. S1 and S2).

Fig. 1 demonstrates that ZapCY1 was fully saturated in the cytosol under resting conditions (i.e., $R_{resting} = R_{max}$), whereas ZapCY2 was only partially saturated. Using ZapCY2, we measured $R_{resting}$, R_{min}, and R_{max} in 16 individual cells and used these parameters to estimate the concentration of free Zn^{2+} in the cytosol to be 80 ± 7 pM (*SI Appendix*, Table S1). This estimate is consistent with previous reports that resting cytosolic concentrations in human colon adenocarcinoma HT-29, HEK 293, and rat insulinoma INS-1(832/13) cells are in the hundreds of picomolar range (5, 22).

Measurement of Zn^{2+} in the ER and Golgi. Because we were unsure whether ER and Golgi Zn^{2+} levels would be higher or lower than the cytosol, the high-affinity ZapCY1 and a low-affinity Zn^{2+} sensor (K_d′ 1 μM), ZifCY1, previously developed in our lab (15) were targeted to lumen of the ER and the inner surface of the Golgi membrane (Fig. 2 *A* and *D*). Colocalization with established ER and Golgi markers confirmed targeting to the desired organelles (*SI Appendix*, Figs. S4 and S5). Treatment with TPEN and Zn^{2+} revealed that both sensors were functional in each of the targeted locations (Fig. 2). TPEN led to a decrease in the FRET ratio for both ER-ZapCY1 and Golgi-ZapCY1 (Fig. 2 *B* and *E*), indicating the presence of free Zn^{2+} in the ER and Golgi. Under the same conditions, no decrease in the FRET ratio was observed for the low-affinity ER-ZifCY1 and Golgi-ZifCY1, likely because the level of Zn^{2+} in ER and Golgi was below the detection limit. Under resting conditions, ZapCY1 was 100% saturated in cytosol, but only 26% saturated in ER and 18% in Golgi, revealing that the labile Zn^{2+} level in ER and Golgi was lower than in cytosol (*SI Appendix*, Fig. S6*A*). To calculate resting Zn^{2+} concentrations in the ER and Golgi, HeLa cells were treated with TPEN to obtain R_{min} and perfused with Zn^{2+} and pyrithione to saturate the sensor and obtain R_{max} (Fig. 2 *B* and *E*). For the ER, thapsigargin was used in combination with TPEN because this aided depletion of the ER. Pseudocolored FRET ratio images of a representative titration are presented in *SI Appendix*, Fig. S3. The free Zn^{2+} in ER ($[Zn^{2+}]_{ER}$) was estimated to be 0.9 ± 0.1 pM and 0.6 ± 0.1 pM in Golgi ($[Zn^{2+}]_{Golgi}$) (*SI Appendix*, Table S1). The dynamic range of the targeted sensors were comparable [ER-ZapCY1, 2.16 ± 0.06 (n = 13 cells, three independent experiments); Golgi-ZapCY1, 2.09 ± 0.07 (n = 13 cells, three independent experiments)], but were lower than that observed in the cytosol. These data demonstrate that the ER and Golgi contain free Zn^{2+} that is buffered at a concentration significantly lower than the cytosol.

Zn^{2+} Sequestration into ER and Golgi. Intracellular Zn^{2+} levels are tightly regulated by transporters and buffering by cytosolic proteins such as metallothionein (2, 22, 23). A fundamental unanswered question is whether organelles sequester zinc, particularly given that there is an excess of high-affinity ligands in the

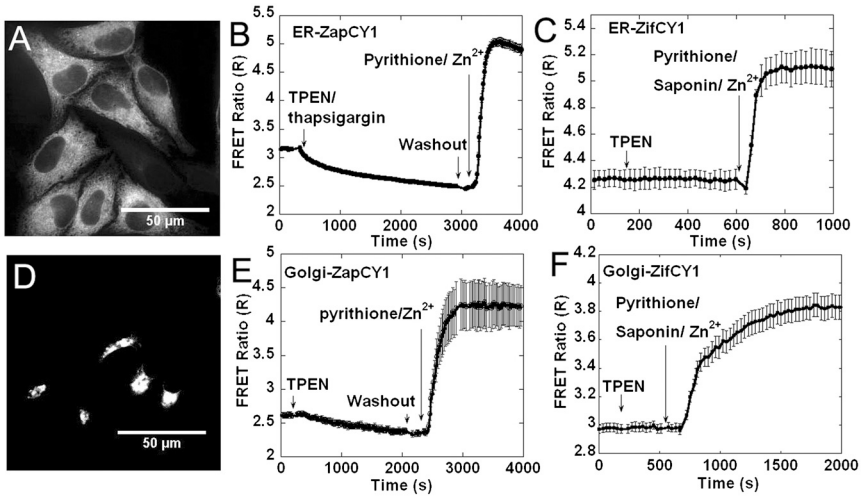

Fig. 2. Targeting Zn^{2+} sensors to ER and Golgi in HeLa cells. (*A*) Fluorescence image of ER-ZapCY1. (*B*) Representative traces ($n = 6$ cells) for ER-ZapCY1. The FRET ratio decreased with 150 μM TPEN/10 μM thapsigargin and increased with addition of 5 μM pyrithione and 10 nM Zn^{2+}. (*C*) Representative traces ($n = 6$ cells) for ER-ZifCY1. The FRET ratio did not change with TPEN but increased with 25 μM pyrithione, 0.001 mg/mL saponin, and 500 μM Zn^{2+}. (*D*) Fluorescence image of Golgi-ZapCY1. (*E*) Representative traces ($n = 4$ cells) for Golgi-ZapCY1. The FRET ratio decreased with 150 μM TPEN and increased with addition of 5 μM pyrithione and 10 nM Zn^{2+}. (*F*) Representative traces for Golgi-ZifCY2 ($n = 7$ cells). The FRET ratio did not change with TPEN but increased with addition of 25 μM pyrithione, 0.001 mg/mL saponin, and 500 μM Zn^{2+}.

cytosol (22). To address this question the plasma membrane was permeabilized with saponin and buffered Zn^{2+} solutions were added to cells. Zn^{2+} uptake was observed with both the high-affinity ER-ZapCY1 and low-affinity ER-ZifCY1, demonstrating that the ER can concentrate high levels of Zn^{2+} (Fig. 3 *A* and *B*). In the Golgi, only Golgi-ZapCY1 detected Zn^{2+} influx, suggesting that the Golgi can concentrate cytosolic Zn^{2+} but to a lower level than the ER (Fig. 3). Next, we explored whether changes in the extracellular environment could affect cytosolic Zn^{2+} levels and organelle sequestration. Fig. 3*C* demonstrates that when 100 μM Zn^{2+} is added to cell media, in the absence of permeabilizing agents, Zn^{2+} is transported into the cytosol, reaching levels of approximately 5.5 nM (*SI Appendix*, Fig. S7). In this experiment, excess Zn^{2+} that accumulates in the cytosol is sequestered into both the ER and Golgi, providing direct evidence that Zn^{2+} is transported into organelles when cytosolic levels reach the nanomolar range. *SI Appendix*, Fig. S11 presents pseudocolor ratio images of the changes in $[Zn^{2+}]_{ER}$ over the time course presented in Fig. 3*C*.

Regulation of ER Zn^{2+} Uptake. To examine the mechanism of Zn^{2+} uptake into the ER, we explored whether the sarco/endoplasmic-reticulum-Ca^{2+}-ATPase (SERCA) was responsible for Zn^{2+} uptake. SERCA is the primary means by which Ca^{2+} is pumped into the ER and Zn^{2+} has been shown to penetrate many Ca^{2+} channels (24), leading us to question whether SERCA could also pass Zn^{2+}. Surprisingly, treatment with a SERCA inhibitor (100 nM thapsigargin) did not inhibit Zn^{2+} uptake, but instead enhanced uptake (Fig. 4*A*). The ER is the main storehouse of Ca^{2+} within the cell and ER Ca^{2+} levels are regulated by SERCA, as well as Ca^{2+} release channels such as the inositol-1,4,5-trisphosphate receptor (IP_3R) and ryanodine receptor (RyR). Inhibition of SERCA causes Ca^{2+} to slowly leak out of the ER, leading to ER Ca^{2+} depletion, elevation of cytosolic Ca^{2+}, and activation of store-operated Ca^{2+} channels to promote influx of Ca^{2+} across the plasma membrane. Thus we next explored whether other agents that perturb ER Ca^{2+} impact ER Zn^{2+} uptake. Cells were treated with histamine which leads to ER Ca^{2+} release through the IP_3R, 2-aminoethoxydiphenyl borate (2-APB) an IP_3R inhibitor, and diltiazem, an L-type Ca^{2+} antagonist and inhibitor of RyR. All reagents were used at standard concentrations known to perturb Ca^{2+} homeostasis (25–27). Both agents (thapsigargin and histamine), which induce release of ER Ca^{2+} into the cytosol, led to enhanced Zn^{2+} uptake, whereas 2-APB which inhibits Ca^{2+} release through the IP_3R did not have a statistically significant effect on Zn^{2+} uptake (Fig. 4*B*). Diltiazem, a RyR inhibitor (27), also gave rise to enhanced Zn^{2+} uptake. At present, we do not have a cohesive explanation for why pharmacological agents with widely different direct impacts on ER Ca^{2+} (two agents promote release, whereas one inhibits release) all enhance Zn^{2+} uptake. However, it is clear that maintenance of ER Ca^{2+} involves a delicately balanced network of processes and perturbation of one component often results in multiple changes in ER Ca^{2+} handling. The pharmacological perturbations presented in this paper do suggest that disruption of the ER Ca^{2+} regulatory network influences Zn^{2+} uptake.

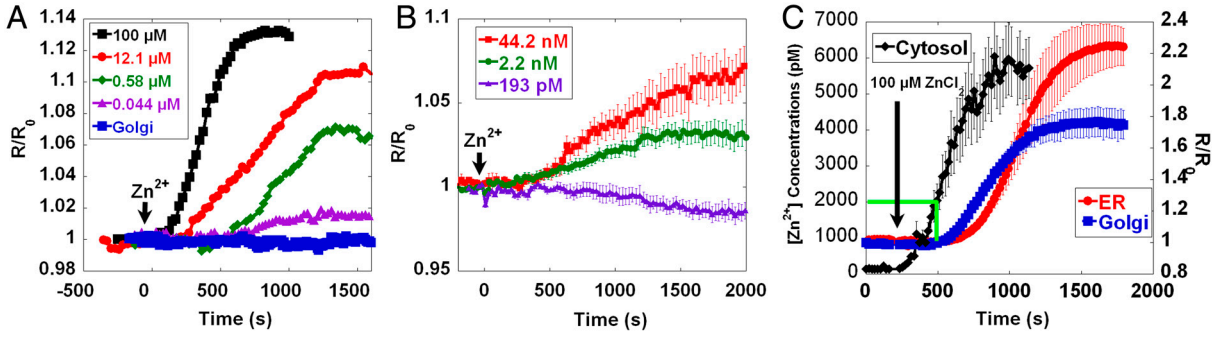

Fig. 3. Comparison of Zn^{2+} uptake in ER and Golgi. (*A*) HeLa cells expressing ZifCY1 targeted to ER and Golgi were permeabilized with saponin for 30 min and then incubated with $ZnCl_2$ (ER: black square, 100 μM, $n = 10$ cells; red circle, 12 μM, $n = 4$ cells; green diamond, 0.58 μM, $n = 4$ cells; violet triangle, 0.044 μM, $n = 7$ cells; and blue square, Golgi, 100 μM, $n = 9$ cells). (*B*) HeLa cells expressing ER-ZapCY1 were permeabilized with saponin for 30 min and then incubated with 193 pM (violet triangle, $n = 4$ cells), 2 nM (green circle, $n = 7$ cells), and 44 nM (red square, $n = 4$ cells) Zn^{2+}. Uptake in ER was recorded as low as 2 nM Zn^{2+}. (*C*) HeLa cells expressing high-affinity Zn^{2+} sensor ER-ZapCY1 ($n = 6$ cells), Golgi-ZapCY1 ($n = 4$ cells), and ZapCY2 were incubated with 100 μM $ZnCl_2$. All Zn^{2+} concentrations below 100 μM were buffered solutions. The left axis represents the cytosolic concentrations whereas the right axis represents the FRET changes in the ER and Golgi.

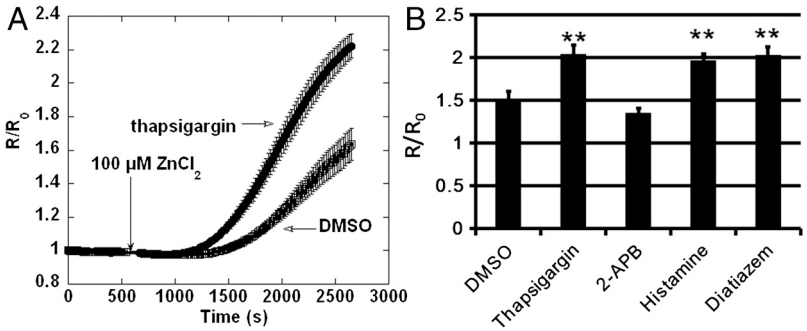

Fig. 4. Regulation of Zn^{2+} uptake in ER. (*A*) Thapsigargin enhanced Zn^{2+} uptake in ER. HeLa cells expressing ER-ZapCY1 sensor were treated with DMSO ($n = 17$ cells, three experiments) or 100 nM thapsigargin ($n = 17$ cells, three experiments) for 5 min (R_0), and then incubated with 100 μM $ZnCl_2$ (R). The relative ratio (R/R_0) indicates the changes of Zn^{2+} in ER. (*B*) Effect of different drugs on Zn^{2+} uptake in ER. HeLa cells expressing ER-ZapCY1 sensors were treated with DMSO ($n = 17$ cells from three experiments), 100 nM thapsigargin ($n = 17$ cells, three experiments), 50 μM 2-APB ($n = 23$ cells, three experiments), 100 μM histamine ($n = 18$ cells from three experiments), or 50 μM diltizem ($n = 17$ cells, three experiments) for 5 min followed by addition of 100 μM $ZnCl_2$ to activate ER Zn^{2+} uptake for 30 min. Compared with DMSO, thapsigargin, histamine, and diltiazem induced greater Zn^{2+} uptake (**$p < 0.01$, ANOVA, Tukey honestly significant difference post hoc test).

To further characterize the connection between Ca^{2+} dynamics and ER Zn^{2+} homeostasis, we explored whether $[Ca^{2+}]_{cyto}$ impacts $[Zn^{2+}]_{ER}$. For these experiments, genetically targeted Ca^{2+} sensors D1ER (28) and D3cpv (29) were used to measure $[Ca^{2+}]_{ER}$ and $[Ca^{2+}]_{cyto}$, respectively. Treatment of HeLa cells with thapsigargin in either the presence or absence of extracellular Ca^{2+} led to Ca^{2+} efflux from ER where reduction of $[Ca^{2+}]_{ER}$ was independent of the extracellular media employed in the experiment (Fig. 5*A*). Calcium efflux from the ER led to rapid elevation of $[Ca^{2+}]_{cyto}$ and a decrease in $[Zn^{2+}]_{ER}$ (Fig. 5 *B* and *C*). ER Ca^{2+} depletion upon thapsigargin treatment activates store-opened Ca^{2+} channels on plasma membrane, which, in the presence of extracellular Ca^{2+}, led to sustained elevation of $[Ca^{2+}]_{cyto}$ and continued decrease in $[Zn^{2+}]_{ER}$ (Fig. 5*B*). On the other hand, in the absence of extracellular Ca^{2+}, $[Ca^{2+}]_{cyto}$ returned back to resting levels and coincident with this $[Zn^{2+}]_{ER}$ increased, possibly as a result of influx from the cytosol (Fig. 5*C*). These perturbations suggest that Ca^{2+} levels in the cytosol influence whether Zn^{2+} is taken up into or released from the ER.

The above experiments all utilized thapsigargin which raises cytosolic Ca^{2+} by inducing release from the ER. To elevate cytosolic Ca^{2+} by an independent means, cells were transfected with the transient receptor potential channel TrpA1. TrpA1 is a cation permeable channel that can be activated by phytochemicals such as mustard oil and cinnemaldehyde (30), and has been shown to transport both Ca^{2+} and Zn^{2+} (31). Treatment of cells expressing TrpA1 with the active ingredient in mustard oil, allyl-isothiocyanate (AITC), led to Ca^{2+} influx across the plasma membrane and concomitant decrease in $[Zn^{2+}]_{ER}$ in accord with the rising $[Ca^{2+}]_{cyto}$ (Fig. 5*D*). Zinc release required the presence of extracellular Ca^{2+} because it did not occur when extracellular Ca^{2+} was absent (*SI Appendix*, Fig. S8). Because Zn^{2+} also acts as an activator for TrpA1 (31), addition of 100 μM extracellular Zn^{2+} in the presence of extracellular Ca^{2+} to HeLa cells expressing

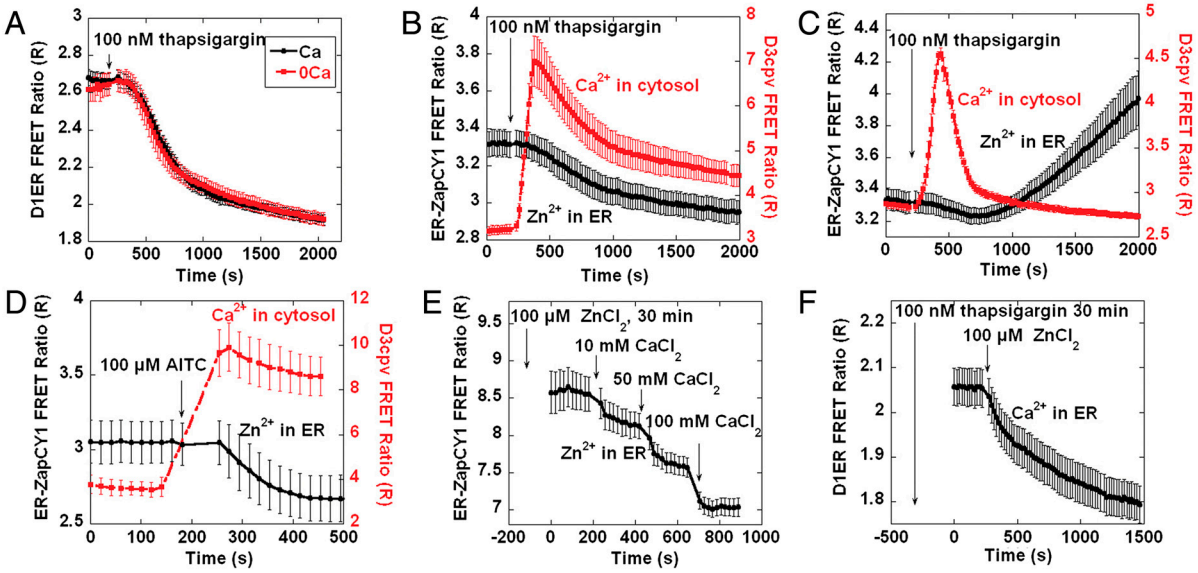

Fig. 5. Ca^{2+} dynamics affect Zn^{2+} homeostasis in the ER. (*A*) Effect of thapsigargin on $[Ca^{2+}]_{ER}$. Treatment with 100 nM thapsigargin, caused $[Ca^{2+}]_{ER}$ to decrease in the presence ($n = 6$ cells) and absence of ($n = 6$ cells) extracellular Ca^{2+}. (*B*) Increasing $[Ca^{2+}]_{cyto}$ reduced $[Zn^{2+}]_{ER}$. Treatment with 100 nM thapsigargin caused $[Ca^{2+}]_{cyto}$ ($n = 5$ cells) to increase; $[Zn^{2+}]_{ER}$ decreased ($n = 6$ cells) concomitantly. (*C*) Thapsigargin increased ER Zn^{2+} when extracellular calcium was absent. $[Ca^{2+}]_{cyto}$ increased ($n = 4$ cells) and then decreased to resting level upon treatment with 100 nM thapsigargin in calcium free Hepes-buffered Hanks Balanced Salt Solution. $[Zn^{2+}]_{ER}$ slightly decreased ($n = 5$ cells) when $[Ca^{2+}]_{cyto}$ increased and then increased when $[Ca^{2+}]_{cyto}$ returned to the resting level. (*D*) Increasing $[Ca^{2+}]_{cyto}$ by activating TrpA1 reduced $[Zn^{2+}]_{ER}$. HeLa cells expressing TrpA1 were treated with AITC, causing $[Ca^{2+}]_{cyto}$ ($n = 4$ cells) to increase and $[Zn^{2+}]_{ER}$ ($n = 4$ cells) to decrease. (*E*) Effects of extracellular Ca^{2+} on $[Zn^{2+}]_{ER}$ ($n = 6$ cells). HeLa cells were preincubated with 100 μM $ZnCl_2$ for 30 min, then increasing extracellular Ca^{2+} reduced $[Zn^{2+}]_{ER}$. (*F*) Effects of extracellular Zn^{2+} on $[Ca^{2+}]_{ER}$ ($n = 5$ cells). HeLa cells were treated with thapsigargin for 30 min to block the SERCA pump. Increasing extracellular Zn^{2+} reduced $[Ca^{2+}]_{ER}$.

TrpA1 also increased $[Ca^{2+}]_{cyto}$ and decreased $[Zn^{2+}]_{ER}$ (*SI Appendix*, Fig. S8). These experiments demonstrate that cytosolic Ca^{2+} fluctuations that arise from ER release or influx across the plasma membrane directly impact ER Zn^{2+} homeostasis.

The connection between Ca^{2+} and Zn^{2+} was further explored by changing extracellular media conditions. HeLa cells were pretreated with 100 μM Zn^{2+} for 30 min to increase the $[Zn^{2+}]_{ER}$ level, and subsequent addition of increasing extracellular Ca^{2+} (10, 50, and 100 mM) caused $[Zn^{2+}]_{ER}$ to decrease in a stepwise fashion (Fig. 5*E*), further demonstrating that cytosolic Ca^{2+} alters $[Zn^{2+}]_{ER}$. To explore whether the cytosolic Zn^{2+} could in turn impact $[Ca^{2+}]_{ER}$, we examined ER Ca^{2+} upon elevation of cytosolic Zn^{2+}. HeLa cells were treated with thapsigargin for 30 min to lower ER Ca^{2+} and prevent refilling of the organelle. Addition of 100 μM $ZnCl_2$ to the extracellular media results in an increase in cytosolic Zn^{2+} to nanomolar levels (Fig. 3*C*), and this stimulus induced release of Ca^{2+} from the ER (Fig. 5*F*). These experiments indicate that elevated cytosolic Ca^{2+} can induce ER Zn^{2+} release and, conversely, elevated cytosolic Zn^{2+} can induce ER Ca^{2+} release.

Discussion

With the growing recognition that labile Zn^{2+} plays important roles in influencing signaling pathways and cellular functions, there has been extensive effort over the past few years to develop fluorescent sensors for monitoring Zn^{2+} fluxes in cells (5, 15, 32, 33). Previously we developed two zinc sensors that utilized a single zinc finger from Zif268 as the sensing module (ZifCY1 $K_d' \sim 1$ μM, ZifCY2 $K_d' \sim 150$ μM) (15). A complementary design based on the copper binding proteins Atox1 and WD4 has also been developed (called eCALWY1-6) with K_d' ranging from 2 pM to 2.9 nM (5). Although the high-affinity sensor (K_d' 2 pM) was sensitive to Cu^{1+}, lower-affinity versions were specific for Zn^{2+}. In this work, we develop ZapCY1, which exhibits high-affinity ($K_d' \sim 2.5$ pM) and selectivity (Fig. 1*C*), and a 4.15-fold dynamic range in the cytosol (approximately twofold in the ER and Golgi); but the dissociation kinetics are slow (Fig. 1*D*). On the other hand, ZapCY2 exhibits faster dissociation kinetics (Fig. 1*E*), a lower Zn^{2+} affinity ($K_d' \sim 811$ pM), reduced selectivity, and a smaller dynamic range (approximately 1.4-fold). The fact that these sensors differ by only two amino acids highlights how difficult it is to predict how sensor properties will be altered by changes in the primary sequence.

Numerous studies have reported measurement of cytosolic free Zn^{2+} in a variety of cell types, including red blood cells (34), leukemic cells (35), splenocytes and thymocytes (36), PC-12 (6), HT-29 (22), HEK 293 (5), INS-1 (832/13) (5), hepatocytes (37), and neurons (38), yielding estimates for resting free Zn^{2+} concentrations from 5 to 1,000 pM. In this paper, we report estimates of free Zn^{2+} in ER and Golgi, which are 0.9 and 0.6 pM, respectively, at least 100 times lower than our estimate of the cytosolic Zn^{2+} concentration (80 pM) in HeLa cells (*SI Appendix*, Table S1).

As suggested by the wide range of reported Zn^{2+} levels, estimates of absolute Zn^{2+} concentration should be regarded with caution. Some discrepancies in Zn^{2+} measurements may reflect true variation in Zn^{2+} levels in different cell types and/or cell state. Indeed in HT29 cells it has been shown that Zn^{2+} levels change with cell state (614 pM in resting vs. 1.25 nM in differentiated cells) (22). However, it is also likely that both the method and nature of the probe influence the absolute estimate. Important considerations include the concentration of the sensor in the cell, potential buffering of endogenous Zn^{2+}, reliability of in situ calibration, and the accuracy of intensity-based vs. ratiometric measurements. For example, the concentration of some small molecule Zn^{2+} sensors has been shown to perturb the sensitivity of the sensor, thus influencing calculation of Zn^{2+} concentrations (39). The most reliable estimates will likely result from measurements in which the sensor minimally perturbs the cellular environment, sensor concentration is minimized, and the K_d' of the sensor is close to the free Zn^{2+} concentration or, better yet, multiple probes with slightly different K_d' values are utilized to constrain the measurements.

In the present study, we explored whether sensor expression level influenced estimates of cytosolic free Zn^{2+} levels by examining the calculated Zn^{2+} concentration as a function of YFP fluorescence intensity. The direct YFP signal does not depend on the presence of Zn^{2+} and hence is an indicator of protein concentration. Over the intensity range examined, we did not see a correlation suggesting that, at the expression levels used in this study, the sensor concentration did not significantly impact our estimates of free Zn^{2+} (*SI Appendix*, Fig. S6). Still, we acknowledge that each sensor has attributes that limit the accuracy of absolute estimates of Zn^{2+}. However, our data clearly provide a reasonable estimate of the *relative* levels of Zn^{2+} in the cytosol, ER, and Golgi. This relative difference is evident using the same sensor (ZapCY1) targeted to different locations where the sensor is 100% saturated in the cytosol but only partially occupied in the ER and Golgi.

In this work, we sought to characterize the role of the ER and Golgi in transporting cytosolic Zn^{2+}. Zn^{2+} uptake into the ER is particularly intriguing because ER function has been shown to depend on Zn^{2+} (17, 18), and the ER plays a central role in integrating cellular signaling events, serving as the hub of Ca^{2+} signaling. Surprisingly we found that Ca^{2+} dynamics influenced ER Zn^{2+} homeostasis and, conversely, that Zn^{2+} could influence ER Ca^{2+} homeostasis. These data suggest a critical link between Ca^{2+} signaling and metal homeostasis. Elevation of cytosolic Ca^{2+} led to ER Zn^{2+} release, whereas elevation of cytosolic Zn^{2+} led to ER Ca^{2+} release, suggesting possible exchange of these two ions across the ER membrane. Given that Ca^{2+} dynamics can be initiated by numerous stimuli and affect a wide range of downstream cellular processes, it will be intriguing to explore whether different Ca^{2+} signaling pathways result in concomitant changes in Zn^{2+} homeostasis.

The electrochemical driving force for movement of ions across the ER membrane can be estimated by considering the difference between the ER membrane potential (V_{ER}) and the equilibrium potential for a given ion (e.g., $E_{Zn^{2+}}$). The equilibrium potential exactly balances the chemical driving force caused by a concentration gradient and can be calculated using the Nernst equation:

$$E_{Zn^{2+}} = \frac{RT}{zF} \ln \frac{[Zn^{2+}]_{cyto}}{[Zn^{2+}]_{ER}}. \quad [1]$$

With our values of $[Zn^{2+}]_{cyto} = \sim 80$ pM and $[Zn^{2+}]_{ER} \sim 0.9$ pM, the $E_{Zn^{2+}}$ for movement of Zn^{2+} from the ER to the cytosol would correspond to $E_{Zn^{2+}} = 58$ mV, whereas movement from the cytosol to the ER would correspond to −58 mV. Currently, there is a dearth of direct experimental evidence for V_{ER}. However, some studies have used theoretical arguments combined with experimental data on Ca^{2+} fluxes from the ER into the cytosol to estimate V_{ER} of neurons (−95 mV) and pancreatic acinar cells (−74 mV) (40). If the V_{ER} of HeLa cells is in a similar range, movement of Zn^{2+} ions from the cytosol into the ER would yield $V_{ER} - E_{Zn^{2+}} = +74$ mV − (−58 mV) = 132 mV. Because the difference in the membrane and equilibrium potential yields a positive value, movement of Zn^{2+} into the ER would be an energetically downhill process ($\Delta G < 0$). However, even if ion movement is energetically favorable, membrane permeability is controlled by channels and pumps, which may need to be activated by a cellular signal (such as increased cytosolic Zn^{2+}). Indeed, our experiments demonstrate that elevation of cytosolic Zn^{2+} above 1 nM induces transport of Zn^{2+} into the ER. Treatment with thapsigargin in the absence of extracellular Ca^{2+} led to more rapid Zn^{2+} uptake, perhaps due to alteration of V_{ER} or

enhanced membrane permeability to Zn^{2+}(activation of a Zn^{2+} channel). Future studies will be aimed at using the genetically encoded sensors developed in this study to identify the protein(s) responsible for this uptake.

Unexpectedly, elevation of cytosolic Ca^{2+} led to release of Zn^{2+} from the ER. Using estimates similar to above, Zn^{2+} release from the ER into the cytosol would correspond to $V_{ER} - E_{Zn^{2+}} = -74\ mV - (58\ mV) = -132\ mV$, an energetically uphill process. Therefore, it is possible this transport is energy dependent. Although, the membrane potential of the ER under this experimental paradigm is likely to be complicated by Ca^{2+} and counterion flux across the ER membrane and is likely changing over the course of the experiment (40, 41).

In conclusion, we have generated two high-affinity genetically encoded sensors for Zn^{2+} and demonstrated that these sensors enable measurement of steady-state Zn^{2+} levels within the ER and Golgi as well as flux of Zn^{2+} into and out of these organelles. Our study reveals a surprising correlation between Zn^{2+} and Ca^{2+} regulation in the ER that suggests potential exchange of these ions across the ER membrane. We suspect that, as the tools for monitoring cellular metals continue to grow, they will help uncover unique connections between metal ions and cellular signaling pathways.

Methods

SI Appendix, Methods includes the design and in vitro characterization of sensors, colocalization protocol, comparison of in vitro and cellular FRET ratios, and methodology for conversion of FRET ratios into Zn^{2+} concentrations.

Cellular Imaging. Sensor constructs were transiently transfected into HeLa cells and imaged in phosphate-free Hepes-buffered Hanks Balanced Salt Solution, pH 7.4, 48 h after transfection. Imaging experiments were carried out on an Axiovert 200 M inverted fluorescence microscope (Zeiss) with a Cascade 512B CCD camera (Roper Scientific), equipped with a Xenon arc lamp (XBO75), and data were collected using Metafluor software (Universal Imaging). Details regarding data collection and processing are presented in *SI Appendix, Methods*.

Statistical Analysis. Statistical analysis was performed using ANOVA with a post hoc test in KaleidaGraph program. Error bars indicate SEM.

ACKNOWLEDGMENTS. We thank Prof. David Eide (University of Wisconin, Madison, WI) for the gift of pFRET-ZnF1/2 and Dr. Ardem Patapoutian (The Scripps Research Institute, La Jolla, CA) for the gift of TrpA1. This work was supported by a Molecular Biophysics Training Grant (National Institutes of Health T32 GM-065103 to P.J.D.), National Institutes of Health Grant (GM084027 to A.E.P.), and The Alfred P. Sloan Foundation (A.E.P.).

1. Takeda A (2000) Movement of zinc and its functional significance in the brain. *Brain Res Brain Res Rev* 34:137–148.
2. Eide DJ (2006) Zinc transporters and the cellular trafficking of zinc. *Biochim Biophys Acta* 1763:711–722.
3. Andreini C, Banci L, Bertini I, Rosato A (2006) Counting the zinc-proteins encoded in the human genome. *J Proteome Res* 5:196–201.
4. Maret W, Krezel A (2007) Cellular zinc and redox buffering capacity of metallothionein/thionein in health and disease. *Mol Med* 13:371–375.
5. Vinkenborg JL, et al. (2009) Genetically encoded FRET sensors to monitor intracellular Zn^{2+} homeostasis. *Nat Methods* 6:737–740.
6. Bozym RA, Thompson RB, Stoddard AK, Fierke CA (2006) Measuring picomolar intracellular exchangeable zinc in PC-12 cells using a ratiometric fluorescence biosensor. *ACS Chem Biol* 1:103–111.
7. Du S, McLaughlin B, Pal S, Aizenman E (2002) In vitro neurotoxicity of methylisothiazolinone, a commonly used industrial and household biocide, proceeds via a zinc and extracellular signal-regulated kinase mitogen-activated protein kinase-dependent pathway. *J Neurosci* 22:7408–7416.
8. Maret W (1995) Metallothionein/disulfide interactions, oxidative stress, and the mobilization of cellular zinc. *Neurochem Int* 27:111–117.
9. Sensi SL, et al. (2003) Modulation of mitochondrial function by endogenous Zn^{2+} pools. *Proc Natl Acad Sci USA* 100:6157–6162.
10. Truong-Tran AQ, Ruffin RE, Zalewski PD (2000) Visualization of labile zinc and its role in apoptosis of primary airway epithelial cells and cell lines. *Am J Physiol Lung Cell Mol Physiol* 279:L1172–1183.
11. Ho LH, Ratnaike RN, Zalewski PD (2000) Involvement of intracellular labile zinc in suppression of DEVD-caspase activity in human neuroblastoma cells. *Biochem Biophys Res Commun* 268:148–154.
12. Kitamura H, et al. (2006) Toll-like receptor-mediated regulation of zinc homeostasis influences dendritic cell function. *Nat Immunol* 7:971–977.
13. Lichten LA, Cousins RJ (2009) Mammalian zinc transporters: Nutritional and physiologic regulation. *Annu Rev Nutr* 29:153–176.
14. Frederickson CJ, Suh SW, Silva D, Thompson RB (2000) Importance of zinc in the central nervous system: The zinc-containing neuron. *J Nutr* 130(Suppl 5):1471S–1483S.
15. Dittmer PJ, Miranda JG, Gorski JA, Palmer AE (2009) Genetically encoded sensors to elucidate spatial distribution of cellular zinc. *J Biol Chem* 284:16289–16297.
16. Atkinson A, et al. (2010) Mzm1 influences a labile pool of mitochondrial zinc important for respiratory function. *J Biol Chem* 285:19450–19459.
17. Ellis CD, et al. (2004) Zinc and the Msc2 zinc transporter protein are required for endoplasmic reticulum function. *J Cell Biol* 166:325–335.
18. Ellis CD, Macdiarmid CW, Eide DJ (2005) Heteromeric protein complexes mediate zinc transport into the secretory pathway of eukaryotic cells. *J Biol Chem* 280:28811–28818.
19. Qiao W, Mooney M, Bird AJ, Winge DR, Eide DJ (2006) Zinc binding to a regulatory zinc-sensing domain monitored in vivo by using FRET. *Proc Natl Acad Sci USA* 103:8674–8679.
20. Miyawaki A, Griesbeck O, Heim R, Tsien RY (1999) Dynamic and quantitative Ca^{2+} measurements using improved cameleons. *Proc Natl Acad Sci USA* 96:2135–2140.
21. Miyawaki A, Tsien RY (2000) Monitoring protein conformations and interactions by fluorescence resonance energy transfer between mutants of green fluorescent protein. *Methods Enzymol* 327:472–500.
22. Krezel A, Maret W (2006) Zinc-buffering capacity of a eukaryotic cell at physiological pZn. *J Biol Inorg Chem* 11:1049–1062.
23. Maret W, Larsen KS, Vallee BL (1997) Coordination dynamics of biological zinc "clusters" in metallothioneins and in the DNA-binding domain of the transcription factor Gal4. *Proc Natl Acad Sci USA* 94:2233–2237.
24. Camello C, Lomax R, Petersen OH, Tepikin AV (2002) Calcium leak from intracellular stores—the enigma of calcium signalling. *Cell Calcium* 32:355–361.
25. Perocchi F, et al. (2010) MICU1 encodes a mitochondrial EF hand protein required for Ca(2+) uptake. *Nature* 467:291–296.
26. Landowski TH, Megli CJ, Nullmeyer KD, Lynch RM, Dorr RT (2005) Mitochondrial-mediated disregulation of Ca^{2+} is a critical determinant of Velcade (PS-341/bortezomib) cytotoxicity in myeloma cell lines. *Cancer Res* 65:3828–3836.
27. Ong DS, Mu TW, Palmer AE, Kelly JW (2010) Endoplasmic reticulum Ca^{2+} increases enhance mutant glucocerebrosidase proteostasis. *Nat Chem Biol* 6:424–432.
28. Palmer AE, Jin C, Reed JC, Tsien RY (2004) Bcl-2-mediated alterations in endoplasmic reticulum Ca^{2+} analyzed with an improved genetically encoded fluorescent sensor. *Proc Natl Acad Sci USA* 101:17404–17409.
29. Palmer AE, et al. (2006) Ca^{2+} indicators based on computationally redesigned calmodulin-peptide pairs. *Chem Biol* 13:521–530.
30. Jordt SE, et al. (2004) Mustard oils and cannabinoids excite sensory nerve fibres through the TRP channel ANKTM1. *Nature* 427:260–265.
31. Hu H, Bandell M, Petrus MJ, Zhu MX, Patapoutian A (2009) Zinc activates damage-sensing TRPA1 ion channels. *Nat Chem Biol* 5:183–190.
32. Que EL, Domaille DW, Chang CJ (2008) Metals in neurobiology: Probing their chemistry and biology with molecular imaging. *Chem Rev* 108:1517–1549.
33. Tomat E, Lippard SJ (2010) Imaging mobile zinc in biology. *Curr Opin Chem Biol* 14:225–230.
34. Simons TJ (1991) Intracellular free zinc and zinc buffering in human red blood cells. *J Membr Biol* 123:63–71.
35. Adebodun F, Post JF (1995) Role of intracellular free Ca(II) and Zn(II) in dexamethasone-induced apoptosis and dexamethasone resistance in human leukemic CEM cell lines. *J Cell Physiol* 163:80–86.
36. Zalewski PD, Forbes IJ, Betts WH (1993) Correlation of apoptosis with change in intracellular labile Zn(II) using zinquin [(2-methyl-8-p-toluenesulphonamido-6-quinolyloxy) acetic acid], a new specific fluorescent probe for Zn(II). *Biochem J* 296:403–408.
37. Brand IA, Kleineke J (1996) Intracellular zinc movement and its effect on the carbohydrate metabolism of isolated rat hepatocytes. *J Biol Chem* 271:1941–1949.
38. Sensi SL, et al. (1997) Measurement of intracellular free zinc in living cortical neurons: Routes of entry. *J Neurosci* 17:9554–9564.
39. Dineley KE, Malaiyandi LM, Reynolds IJ (2002) A reevaluation of neuronal zinc measurements: Artifacts associated with high intracellular dye concentration. *Mol Pharmacol* 62:618–627.
40. Burdakov D, Petersen OH, Verkhratsky A (2005) Intraluminal calcium as a primary regulator of endoplasmic reticulum function. *Cell Calcium* 38:303–310.
41. Jafri MS, Gillo B (1994) A membrane potential model with counterions for cytosolic calcium oscillations. *Cell Calcium* 16:9–19.